Trends in Nano- and Micro-Cavities, 2011, 109-152

Chapter 4

Review on unidirectional light emission from ultralow-loss modes in deformed microdisks

Jan Wiersig*, Julia Unterhinninghofen

Institut für Theoretische Physik, Universität Magdeburg,
Postfach 4120, D-39016 Magdeburg, Germany
e-mail: jan.wiersig@ovgu.de

Qinghai Song, Hui Cao

Department of Applied Physics, Yale University,
New Haven, CT 06520-8482, USA

Martina Hentschel, Susumu Shinohara

Max-Planck-Institut für Physik komplexer Systeme,
Nöthnitzer Str. 38, D-01187 Dresden, Germany

***Corresponding Author**

O'Dae Kwon, Byoungho Lee and Kyungwon An (Eds)

Abstract

In microdisk cavities, whispering-gallery optical modes are confined by total internal reflection at the boundary of the disk. The small mode volumes and the ultralow losses of the modes offer a high potential for several applications, such as low-threshold lasing. The uniform in-plane light emission from an ideal disk with circular cross section, however, is a significant drawback. In this chapter we review the recent progress in microdisk design for unidirectional light emission from modes with low losses. We compare and discuss the pros and cons of various approaches. One important aspect is the ray-wave correspondence in such deformed microdisks.

Contents

1 Introduction

The confinement of photons in all three spatial dimensions using microcavities has triggered intense basic and applied research in physics over the past decade [1]. As some examples we mention the research on low threshold lasing [2, 3], single-photon emitters [4], and solid-state cavity quantum electrodynamics [5–8]. Important realizations of optical microcavities are whispering-gallery cavities such as microdisks [9–12], microspheres [13–15], and microtoroids [16–18] which trap photons for a long time τ near the boundary by total internal reflection. The corresponding whispering-gallery modes (WGMs) have very high quality factors $Q = \omega\tau$, where ω is the resonance frequency. The record Q value in this case is around $7 \cdot 10^5$ for semiconductor [10] and $6 \cdot 10^7$ for silica microdisks [11]. The high quality factors and the in-plane light emission make microdisks attractive candidates for several optoelectronic devices, especially for material systems where other cavity designs such as vertical-cavity surface-emitting laser (VCSEL) micropillars face severe challenges in the fabrication [19]. Unfortunately, the possible use of microdisks is limited by the fact that the in-plane light emission is isotropic as illustrated in Fig. 1(a).

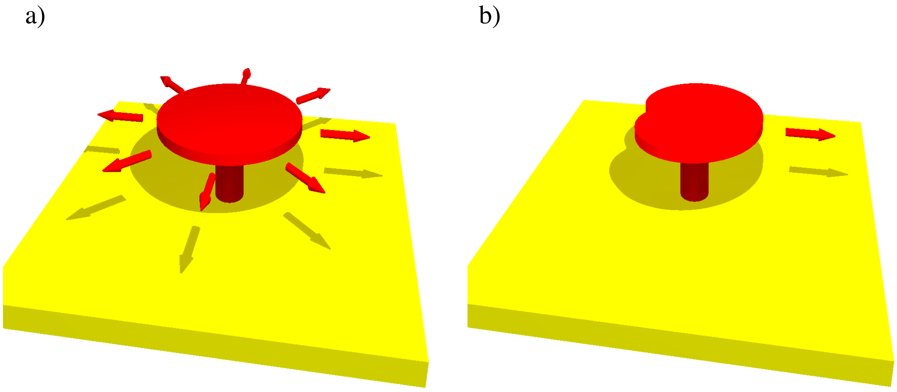

Figure 1: Illustration of a circular (a) and a deformed (b) microdisk cavity supported by a pedestal. The arrows indicate the direction of light emission.

Figure 1(b) sketches the possibility to improve the directionality of light emission by deforming the boundary of the cavity [20–23]. Several deformations have been proposed and realized, see for example the cavities in Fig. 2. But only a few shapes discussed in the literature lead to light emission into a single direction with reasonable angular divergence [24–26] that is essential for many applications. Moreover, several of these deformed microdisks suffer from Q spoiling [27]: The quality factor degrades dramatically upon deformation, in the worst case ruling out any application. The trade-off between quality factor and directionality is not only a problem of microdisks but also of microspheres, microtoroids, and even of VCSEL-micropillars; for a given total number of Bragg mirror pairs a micropillar can be optimized either w.r.t. the quality factor (roughly equal number of bottom and top mirror pairs) or directionality (otherwise).

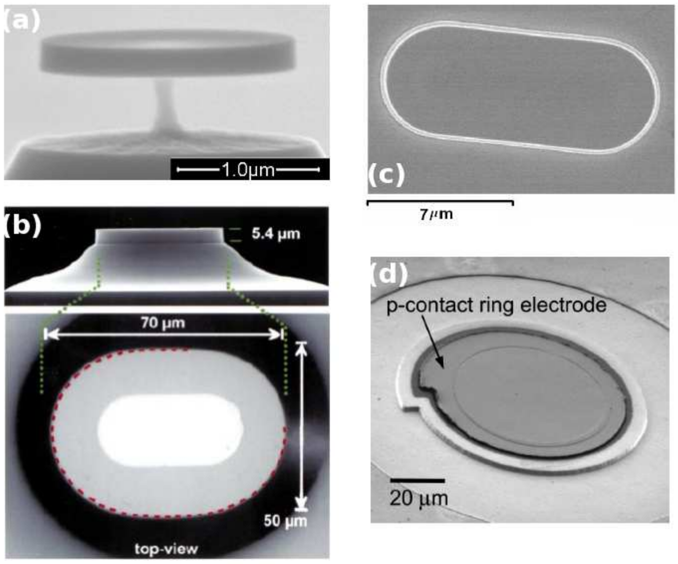

Figure 2: Scanning electron microscope (SEM) images of a few microcavities. (a) Tilt view of a circular GaAs disk on top of an AlGaAs pedestal. (b) Side and top view of a flattened quadrupolar shaped GaAs cylinder [22]. (c) Top view of a polymer (PMMA) disk of stadium shape. (d) Top-view of an InGaN spiral microcavity with a ring-shaped p-contact electrode [26].

The aim of this chapter is to review the progress in achieving unidirectional light emission from deformed microdisks. The paper is organized as follows. In Section 2 we discuss the relationship between boundary shape deformations and ray dynamical chaos. Sections 3-8 provide an overview over the different approaches to get unidirectional light emission. Wavelength-scale microdisks are discussed in Section 9. Finally, Section 10 contains the summary.

2 Shape deformation and ray chaos

Microdisk cavities can be modelled as quasi-two-dimensional systems with piece-wise constant effective index of refraction $n(x, y)$. In this case Maxwell's equations reduce to a two-dimensional scalar mode equation [28]

$$-\nabla^2\psi = n^2(x,y)\frac{\omega^2}{c^2}\psi \ , \tag{1}$$

with frequency $\omega = ck$, wave number k, and the speed of light in vacuum c. The mode equation (1) is valid for both transverse magnetic (TM) and transverse electric (TE) polarization. For TM polarization the electric field $\vec{E}(x,y,t) \propto (0,0,\mathrm{Re}[\psi(x,y)e^{-i\omega t}])$ is perpendicular to the cavity plane. The wave function ψ and its normal derivative are continuous across the boundary of the cavity. For TE polarization, ψ represents the z-component of the magnetic field vector H_z. Again, the wave function ψ is continuous across the boundaries, but its normal derivative $\partial_\nu\psi$ is not. Instead, $n(x,y)^{-2}\partial_\nu\psi$ is continuous [28]. At infinity, outgoing wave conditions are imposed which results in quasi-bound states with complex frequencies ω in the lower half-plane. Whereas the real part is the usual frequency, the imaginary part is related to the lifetime $\tau = -1/[2\,\mathrm{Im}\,\omega]$ and to the quality factor $Q = -\mathrm{Re}\,\omega/[2\,\mathrm{Im}\,\omega]$.

In general, the optical modes in microcavities cannot be computed analytically. Over the last decades, several numerical schemes have been therefore developed for the calculation of optical modes. Finite-difference time-domain (FDTD) methods [29] are well suited to model light propagation through microstructures [30]. It has also been used to find the resonances of microcavities and the lasing modes [31–33]. However, the calculation of optical modes with high quality factors requires long computation times. For this reason it is often more convenient to work directly in the frequency domain. Another advantage is that a frequency-dependent index of refraction can be easily included. Available methods are wave matching [34], boundary element methods [35–37] and volume element methods [38–41]. Figure 3 shows as an example a mode in a microdisk with the shape of a stadium given by two semicircles and two parallel segments; see also Fig. 2(c).

From the complex spatial mode pattern in Fig. 3 it becomes apparent that it is desirable to not only compute the modes but also to understand their relevant features. This is of high practical value for the development of novel cavity designs. It turns out that much understanding about the wave dynamics in microcavities can be gained by studying the ray-wave correspondence [21,42]. This is in analogy to studying the quantum-classical correspondence in the field of quantum chaos [43–46].

A frequently studied class of model systems in nonlinear dynamics and quantum chaos are planar billiards, see, e.g., Refs. [47–56]. In a classical billiard a point-like particle moves freely in a two-dimensional plane domain

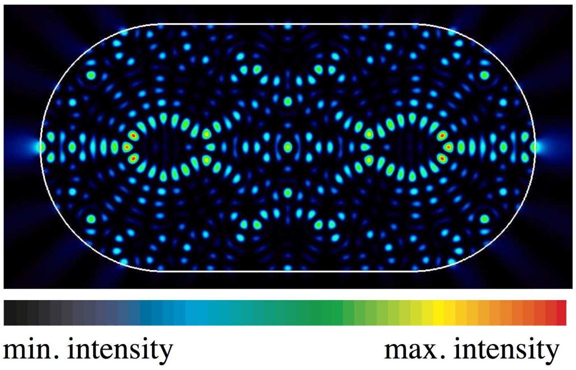

Figure 3: Calculated near-field intensity pattern of an optical mode in a semiconductor microstadium. Intensity is higher for redder colors, and vanishes in the dark regions. The refractive index inside the cavity is $n = 3.3$ and outside $n = 1$. Note the light intensity outside the cavity.

with elastic reflections at a hard boundary. The character of the dynamics is controlled by the shape of the boundary curve. Figure 4 illustrates as an example the stadium billiard [57]. A typical pair of trajectories with very similar initial conditions is shown. After a few reflections the two trajectories have completely separated from each other. This sensitive dependence on initial conditions obviously destroys the long-term predictability. Fully chaotic systems, such as the stadium billiard, exhibit this sensitivity for almost all pairs of initial conditions. The other extreme case is the class of integrable billiards, such as the circular billiard, which show regular dynamics without sensitive dependence on initial conditions. Generic billiards are partially chaotic, i.e., chaotic and regular motion coexist in phase space [47]. These systems are often referred to as “systems with mixed phase space”.

For a classical billiard the associated quantum billiard is defined by the free single-particle Schrödinger equation with wave functions that vanish on and outside the boundary of the same domain. In general, such an infinite-potential-well problem cannot be solved by means of separation of variables. Note that as the Schrödinger equation is linear, it cannot possess exponential instability in time as do the classical equations of motion. Understanding the quantum mechanical implications of classical chaos is the main issue in the field of quantum chaos [43–46]. A fundamental tool used in this field to study the quantum-classical correspondence of fully and partially chaotic systems is the so-called semiclassical approximation, which is an expansion in terms of the small but finite wavelength divided by a characteristic length

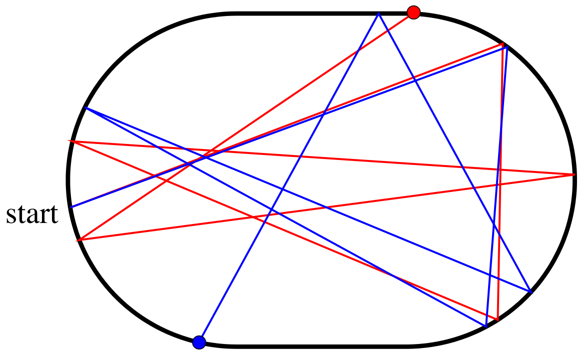

Figure 4: Chaos in the stadium billiard: two classical trajectories starting at the same position but with slightly different initial direction separate from each other after a few elastic reflections at the boundary.

scale. The semiclassical approximation still contains quantum effects like interference.

In the quasi-2D approximation the mode equation (1) for a microdisk corresponds to the time-independent Schrödinger equation of a quantum billiard with the same boundary curve if the electromagnetic field is identified with the quantum mechanical wave function. Correspondingly, light rays can be identified with classical trajectories. However, there is a fundamental difference between an optical microdisk and a quantum billiard. The boundary conditions of a dielectric cavity imply leakage of light. Hence optical microdisks represent a realization of open billiards [21,34]. These systems offer the possibility to investigate the *ray-wave correspondence of open systems* in connection with experiments and applications. It is worth to mention that not only deformed microdisks are interesting for quantum chaos but also other cavity geometries such as vertical-cavity surface-emitting lasers (VCSELs) [58, 59] and deformed microspheres [60, 61].

In the first experiments on microdisks, circular-shaped disks have been studied [9,62,63] because they provide the largest quality factors. Figure 5(a) illustrates a ray trajectory in a circular microdisk with radius R trapped by total internal reflection. The corresponding modes are called whispering-gallery modes named after the whispering gallery at the St. Paul's Cathedral in London. There, Lord Rayleigh analyzed propagation of acoustic waves [64].

A deeper understanding of the ray dynamics in microdisks can be acquired through a study of the phase space of the corresponding closed billiard system. The phase space is four dimensional consisting of two spatial degrees of freedom and two conjugate momenta. But due to conservation of the modulus of the momentum, the motion actually takes place on a three-dimensional surface. A powerful tool in the field of nonlinear dynamics to investigate the dynamics on such a surface is the so-called Poincaré surface of section (SOS) [65]. It is a plot of the intersection points of a set of trajectories with a surface in phase space. For the trivial case of the circular billiard the SOS is illustrated in Fig. 5(a). Starting with a given trajectory, its position in terms of the arclength coordinate along the circumference s and the quantity $\sin\chi$ are recorded always directly after the particle is reflected at the billiard's boundary. With the total momentum being normalized to unity, $\sin\chi \in [-1, 1]$ can be interpreted as tangential momentum component with respect to the boundary curve at the position $s \in [0, s_{\max}]$. We adopt the convention that $\sin\chi > 0$ means counterclockwise rotation and $\sin\chi < 0$ means clockwise rotation. The so-called Birkhoff coordinates $(s, \sin\chi)$ are the most natural representation of a Poincaré SOS for billiard systems as the map from bounce to bounce, $(s_i, \sin\chi_i) \to (s_{i+1}, \sin\chi_{i+1})$, is area-preserving [47].

In the case of the integrable circular billiard, the conserved angular momentum is proportional to $\sin\chi$. Hence rays are confined to two-dimensional surfaces of constant $\sin\chi$ and constant modulus of the momentum. The topology of such invariant surfaces is that of a two-dimensional torus [66]. The confinement on lower-dimensional surfaces has important consequences for the open circular microdisk. Consider a ray that initially fulfills the condition for total internal reflection $|\sin\chi| > 1/n$, see red line in Fig. 5(a). Since the ray does not leave the invariant torus $\sin\chi = \text{const}$, it cannot enter the leaky region between the two critical lines for total internal reflection $\sin\chi_c = \pm 1/n$. Hence, such a ray never leaves the cavity as long as wave effects like evanescent leakage, the optical analogue of quantum tunneling, are ignored.

The rotational symmetry of a circular microdisk results in an uniform far-field emission pattern, which is a considerable disadvantage for most applications, in particular for microlasers. Breaking the rotational symmetry, e.g., by deforming the boundary, leads in almost every case to an open billiard with partially or fully chaotic ray dynamics and an improved far-field emission pattern [21–23,67–69]. To illustrate the ray dynamics in a deformed microcavity, we consider a specific boundary curve, the limaçon of Pascal which reads in polar coordinates (ρ, ϕ)

$$\rho(\phi) = R(1 + \varepsilon\cos\phi) \ . \tag{2}$$

The limiting case of vanishing deformation parameter ε is the circle. The corresponding family of closed cavities is known as "limaçon billiards" [49, 50].

According to Refs. [27,49,70] the limaçon billiard with small perturbation parameter ε obeys the Kolmogorov-Arnol′d-Moser (KAM) theorem [71–73]. It states that for a sufficiently smooth perturbation of an integrable system some of the invariant tori survive, while others are destroyed giving rise to partially chaotic dynamics. Figure 5(b) shows that in this situation new regions, the "regular islands", appear. The centre points of these islands host stable periodic trajectories. Figure 5(c) shows the case of a stronger perturbation where the phase space is mixed. It shows regular islands in the "chaotic sea". A trajectory starting in this region diffuses in phase space in a chaotic fashion as indicated by the small black dots. The remaining regular islands disappear more and more as the deformation parameter is further increased; see Fig. 5(d).

The discussed phase-space structure of the closed billiard has consequences for the ray dynamics of the open microcavity. A typical ray trajectory in a strongly deformed cavity as shown in Fig. 5(d) starting with an initial $\sin\chi$ well above the critical line, follows the chaotic diffusion such that it rapidly enters the leaky region where it escapes according to Snell's and Fresnel's laws. From this observation one would conclude that modes in chaotic microdisks have low Q-factors. This Q spoiling [27, 34] would limit the possible applications of deformed microdisks considerably. However, wave localization effects discovered in the field of quantum chaos provide the possibility of high-Q modes in chaotic cavities. For example, wave packets mimic to some extent the chaotic ray diffusion. However, destructive interference suppresses the chaotic diffusion on long time scales [74, 75]. This phenomenon is called dynamical localization to place emphasis on the dynamical aspect. As a side remark we mention that dynamical localization is closely related to Anderson localization in disordered solids [74]. Dynamical localization has been demonstrated for microdisks with enhanced surface roughness [76–78]. Another wave localization phenomenon is scarring [79]. It refers to the existence of a small fraction of quantum eigenstates with strong concentration along unstable periodic trajectories of the underlying classical system. In optical microcavities, this localization of wave intensity has been observed in theory and experiment [31–33, 80–83].

In cavities with a mixed phase space, diffusion can be significantly less pronounced than in fully chaotic systems; cf. Figs. 5(c) and (d). This is due to the presence of dynamical barriers (complete or partial barriers) in phase space. Examples are regular regions, which cannot be penetrated by chaotic ray trajectories. Here, wave effects like dynamical tunneling can effectively enhance the diffusion. Dynamical tunneling is a generalization of conventional tunneling which allows one to pass not only through an energy barrier but also through other kinds of dynamical barriers in phase space [84]. The effect of dynamical tunneling in microcavities has been discussed in Refs. [61, 85–87]. Tunneling between regular islands that are separated in phase space by a chaotic sea is called chaos-assisted tunneling [54, 88, 89]. It has been demonstrated that the quality factors and the directionality of the light emission from microcavities can be strongly influenced by chaos-assisted tunneling [90].

This zoo of ray and wave dynamical effects is itself interesting enough to be studied. In this review, we focus on the usage of ray-wave correspondence to achieve unidirectional light emission from microdisks.

3 Spiral

Spiral microcavity lasers, such as the one in Fig. 2(d), have early been considered as a candidate for directional emission [26, 91]. In polar coordinates the boundary of the spiral cavity is defined as

$$\rho(\phi) = R\left(1 + \frac{\varepsilon}{2\pi}\phi\right) \tag{3}$$

with deformation parameter $\varepsilon \geq 0$ and "radius" $R > 0$ at $\phi = 0$. The radius jumps back to R at $\phi = 2\pi$ creating a notch. The (too) simple idea was that the symmetry breaking end of the spiral, the so-called notch, induces the outcoupling of the counter-clockwise propagating modes that approach the notch, see Fig. 6(a), that would be WGMs in the unperturbed disk. An easy argument against this mechanism is that pairs of clockwise and counter-clockwise modes do not exist in the spiral [92, 93]. We therefore speak in the following about clockwise and counter-clockwise propagating waves instead of modes. The lifetime of such a counter-clockwise propagating wave is, in the spiral, lower than the one of its clockwise-propagating complement that does not see the notch. Therefore, it should not be relevant for lasing, and the lasing operation should be carried by the clockwise-propagating waves (that remain similar to WGMs). Indeed, experiments [94] on quantum cascade lasers found no directional emission as was supported by ray and wave simulations [95, 96]. This situation is depicted in Fig. 6(b): The long-lived WG-type waves dominate the emission characteristics that exists of a number of spikes originating from those waves and leaving the cavity with the respective sense of rotation. They explain the spiky far-field pattern that was observed in the experiments [94] and are consistent with wave simulation and the chaotic ray dynamics of the spiral [95, 96].

Despite the convincing agreement between experiment, ray, and wave simulations, these results contradict earlier results [26, 91] that actually had confirmed a directional light output from spiral-shaped microcavities. A closer look reveals one important difference in the experimental setups: Whereas the above-mentioned, later experiments used uniformly pumped microcavities, the earlier experiments were all based on boundary-pumped schemes [91] (the pumped area is denoted by the yellow color in Fig. 6). In fact, this boundary pumping was found to be a crucial prerequisite for achieving directional emission, though it was not included in the theoretical explanation given in the same paper [91].

More recent calculations [97] for active, i.e. lasing, spiral-shaped microcavities based on the Schrödinger-Bloch model show that boundary pumping is indeed essential, cf. Fig. 6(c). These simulations revealed that directional emission from boundary-pumped spiral microlasers relies on an intricate mode-beating mechanism that is made possible by effectively enlarging the lifetime of the short-lived counter-clockwise propagating waves through the boundary pumping. As a result, the lifetime becomes similar to that of the clockwise-propagating wave – a precondition for enabling the mode-beating mechanism. As a consequence of this intricate wave dynamics, the directional light output occurs in a pulsed manner with an overall laser threshold that is somewhat higher than in other schemes presented in this review.

Based on these simulations, a statement about the size of the notch that optimizes the directionality was also obtained: It should be about two wavelengths – i.e., sufficiently large to break the circular symmetry, but at the same time small enough to ensure the best possible light confinement. The light emission from the notch occurs in an angle of approximately 45 degree with respect to the notch line.

4 Rounded triangle

In Ref. [25] a microcavity with the shape of a rounded isosceles triangle was proposed for unidirectional light emission. The directionality has been demonstrated by numerical computation of optical modes and stationary lasing pattern based on the Schrödinger-Bloch model [98, 99]. The geometry and a stationary lasing pattern are depicted in Fig. 7. The reason for the directionality is that the rounded part on the left hand side forms a whispering-gallery-type of mode pattern, which implies that a significant portion of light intensity is reflected on this part of the cavity. Therefore, the light has to escape predominately on the right part leading to unidirectional emission.

Even though the near-field pattern in Fig. 7 looks quite promising, this particular geometry has three disadvantages. First, the actual far-field pattern has a rather large divergence angle of about 90 degree. Second, the directionality was only observed numerically for low size parameters kR, where R here is the maximum diameter of the cavity. The directionality was not present in experiments with larger size parameters [100]. Third, and most importantly, the quality factor is very small, about 35. This low quality factor rules out most applications in photonics and optoelectronics.

5 Space Capsule

Schwefel and Stone designed space-capsule shaped cavities depicted in Fig. 8(a) and explored the possibility of obtaining unidirectional output [101]. Two specially designed cavity boundaries, called D1 and D2, can be described as

$$\rho = R(1 - 0.013 \cos 2\phi + 0.0888 \cos 3\phi) \ ,$$

and

$$\rho = R(1 - 0.02 \cos 2\phi + 0.072 \cos 3\phi) \ .$$

These two cavities have only one symmetry axis. The stable orbit modes have two output points and only one beam direction. For example, the D1 cavity has only one dominant stable orbit present in the SOS [Fig. 8(b)]. This is a triangle orbit with three bounces. For a GaN disk, two bounce points are close to the critical line in the SOS. They serve as the output portals emitting in the same direction.

With uniform pumping across the cavity (flood pumping), the stable orbit should support lasing. Experimentally, the pump intensity and the beam quality were not sufficient for flood pumping of the GaN disks of D1 and D2 shapes ($R = 100, 300, 500\mu$m). Instead an axicon lens was used to focus the pump light to a ring on the disk and excite the whispering gallery modes. The emission occurs at the three corners, producing output in three directions.

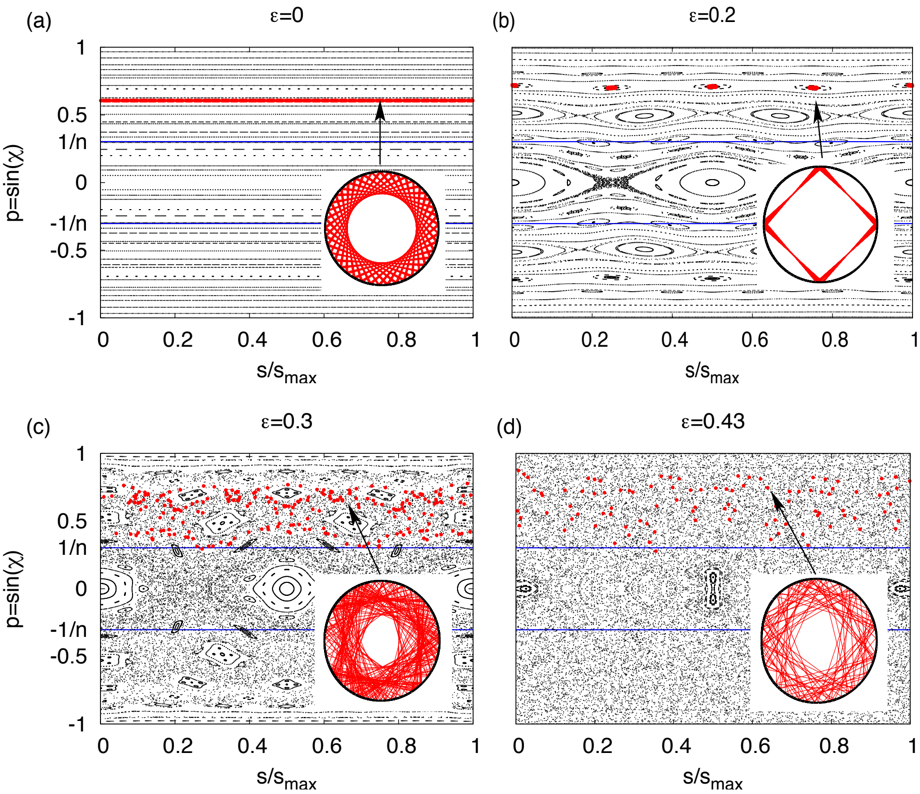

Figure 5: (a) Circular microdisk: whispering-gallery ray trajectory (red) in real space and in the Poincaré surface of section; s is the arclength coordinate and χ is the angle of incidence. The critical lines $\sin\chi_c = \pm 1/n$ (blue) enclose the leaky region where the condition for total internal reflection is not fulfilled. Typical trajectories in the circular billiard fill a line of constant $\sin\chi$ (black lines). Poincaré surface of section of limaçon cavity defined in Eq. (2) with $\varepsilon = 0.2$ (b), $\varepsilon = 0.3$ (c), and $\varepsilon = 0.43$ (d).

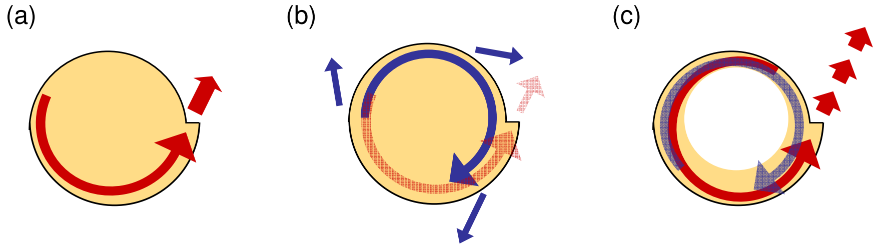

Figure 6: Directional emission from spiral microlasers. (a) Oversimplified scheme to achieve directionality by breaking the rotational symmetry with the notch. (b) The reason that this scheme does not work in uniformly pumped spiral microcavities is the short lifetime of these counter-clockwise propagating waves denoted by the red arrow in (a) - the one of the clockwise propagating WG-type waves (blue arrow) is higher. (c) Directional emission can, however, be made possible by boundary pumping that effectively amplifies the lifetime of the counter-clockwise propagating waves that see the notch, resulting in a mode-beating mechanism with the clockwise propagating WG-type waves that yields a pulsed directional emission from the notch under approximately 45 degrees.

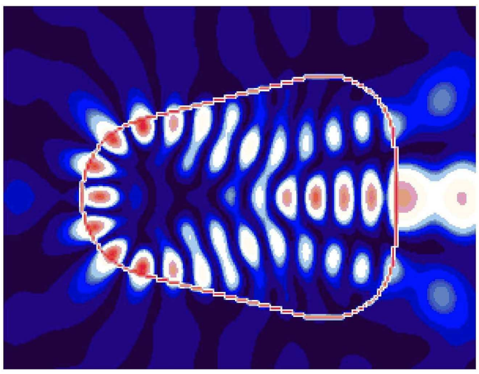

Figure 7: Stationary lasing near-field pattern in the rounded isosceles triangle with refractive index $n = 2$. The electromagnetic field is TM polarized. Reprinted from Ref. [25] with kind permission from Optics Letters.

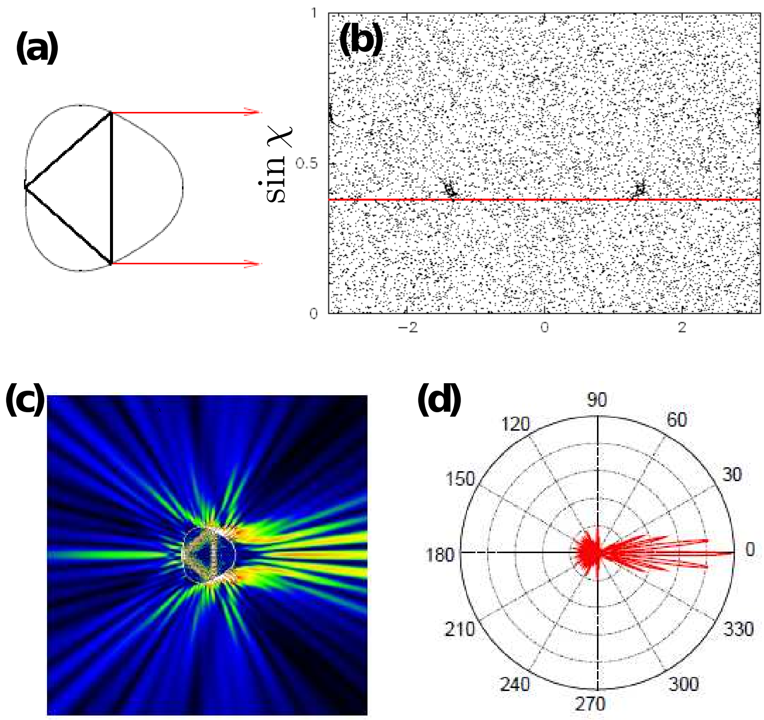

Figure 8: (a) Triangular orbit in the D1 cavity, with output in one direction. (b) The surface of section (SOS) for the D1 cavity showing only one stable periodic orbit as drawn in (a). (c, d) Real-space intensity distribution (the outside and inside field intensities are individually scaled for display purpose) and far-field emission of a cavity mode based on the dominant stable triangular orbit. $kR = 30.1808 - 0.01388i$. The Q factor is 4349.

6 Internal WGMs

In this paragraph we discuss another interesting approach based on the construction of cavities with continuous families of periodic orbits [102]. Such a cavity can support invariant lines of whispering-gallery type above the critical line of total internal reflection but below the region of conventional whispering-gallery trajectories. These "interior WGMs" predominately emit by tunneling into the leaky region. Provided that the invariant line has a sufficient asymmetric shape in phase space, this mechanism can lead to directional or even undirectional emission.

Figure 9 demonstrates that this concept can indeed be used to get optical modes in a deformed microdisk which has emission mainly into a single direction. Unfortunately, there is no statement about the quality factor in this particular case [102]. For bidirectional emission theoretical (experimental) quality factors around 10^4 (6000) are reported [103].

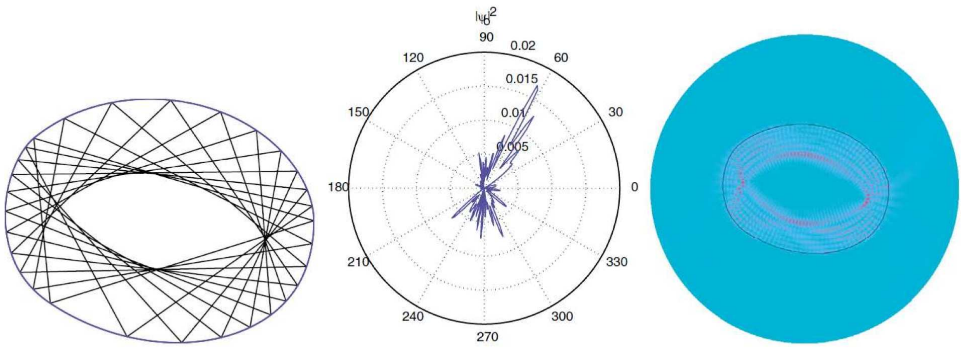

Figure 9: Family of interior whispering-gallery type trajectories (left), corresponding far field distribution (middle) and internal mode pattern (right). The index of refraction is $n = 3$. Reprinted from Ref. [102] with kind permission from Physical Review Letters.

Apart from the difficulty of finding such a constant width curve this approach has another, more serious problem, namely the coexistence of interior and conventional WGMs. The latter have higher quality factors as the distance from the leaky region is larger. In the case of flood pumping, the conventional WGMs lase first due to lower threshold, producing nondirectional output. Carrier injection to the cavity center selects internal WG modes for lasing because they have better spatial overlap with the gain region. This selective pumping method, however, is difficult to implement for microcavities of dimension less than 5 μm.

Another way to suppress the lasing of conventional WGMs is to deliberately introduce surface roughness. As the conventional WGMs are located closer to the boundary of the cavity than the interior ones, the quality factor of the conventional WGMs will suffer more strongly from the Q-spoiling due to surface roughness. In this way the quality factors of the conventional WGMs can be made slightly smaller than those of the interior ones [103]. Obviously, this approach limits the achievable quality factors and is therefore not favorable.

7 Mode coupling

In this section we discuss a scheme which overcomes the trade-off between quality factor and directionality by combining dynamical tunneling and refractive escape [104]. The idea is to couple a uniform high-Q mode (HQM) and a directional low-Q mode (LQM) using enhanced dynamical tunneling near avoided resonance crossings. Such avoided crossings appear in open systems, where a complex frequency is assigned to each mode. Avoided resonance crossings are generalizations of avoided frequency (or energy level) crossings. Avoided level crossings in closed or conservative systems are discussed in textbooks on quantum mechanics. They occur when the curves of two energy eigenvalues, as function of a real parameter Δ, come near to crossing but then repel each other [105]. This behavior can be understood in terms of a 2×2 Hamiltonian matrix

$$H = \begin{pmatrix} E_1 & V \\ W & E_2 \end{pmatrix} . \tag{4}$$

For a closed system this matrix is Hermitian, thus the energies E_j are real and the complex off-diagonal elements are related by $W = V^*$. The eigenvalues of the coupled system,

$$E_{\pm}(\Delta) = \frac{E_1 + E_2}{2} \pm \sqrt{\frac{(E_1 - E_2)^2}{4} + VW} , \tag{5}$$

differ from the energies of the uncoupled system E_j only in a narrow parameter region where the detuning from resonance, $|E_1(\Delta) - E_2(\Delta)|$, is smaller or of the size of the coupling strength $\sqrt{VW}$. The parameter dependence of V and W can often be safely ignored.

The matrix (4) also captures features of avoided *resonance* crossings in open or dissipative systems if one allows for complex-valued energies E_j. The imaginary part determines the lifetime $\tau_j \propto 1/\mathrm{Im}(E_j)$ of the quasi-bound state far away from the avoided crossing $|E_1 - E_2|^2 \gg VW$, where the off-diagonal coupling can be neglected. Keeping the restriction $W = V^*$ allows for two different kinds of avoided resonance crossings [106] as illustrated in Fig. 10. For the strong coupling situation $|V| > V_c = |\text{Im}(E_1) - \text{Im}(E_2)|/2$, there is an avoided crossing in the real part of the energy and a crossing in the imaginary part upon which the eigenstates interchange their identity. Correspondingly, all spatial mode characteristics such as, e.g., the far-field patterns switch their identity. At resonance $\text{Re}(E_1) = \text{Re}(E_2)$ the eigenvectors of the matrix (4) are symmetric and antisymmetric superpositions of the eigenvectors of the uncoupled system. If one of the latter corresponds to a localized state then such an avoided crossing leads to delocalization and lifetime shortening [107]. For the weak coupling situation $|V| < V_c$, there is a crossing in the real part and an avoided crossing in the imaginary part. Here, the eigenstates, and also the spatial mode characteristics, do not interchange but only intermix near the crossing point. Moreover, the quality factors are roughly maintained.

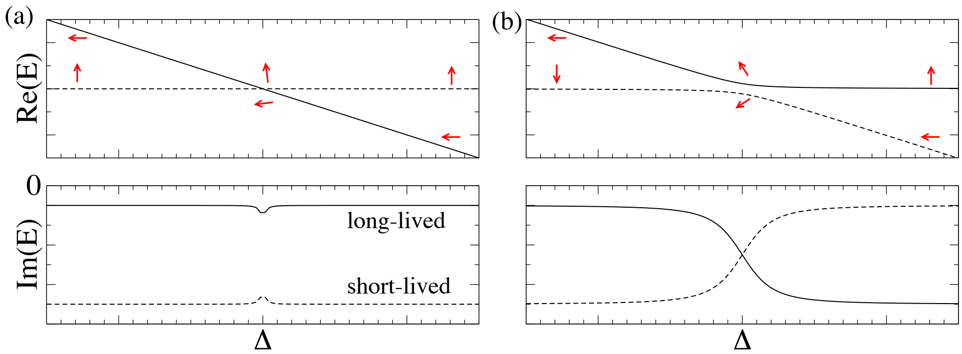

Figure 10: Avoided resonance crossing of the eigenvalues of the matrix in Eq. (4) in the weak coupling regime $|V| < V_c$ (a) and in the strong coupling regime $|V| > V_c$ (b) calculated from Eq. (5). Arrows schematically indicate the behaviour of the corresponding eigenvectors demonstrating the hybridization near the avoided crossing.

The general idea is to exploit the weak coupling scenario to slightly "hybridize" a HQM and a directional LQM to a mode with high quality factor and the directed far-field pattern of the LQM. This scheme can be realized in three steps. First, take a cavity with HQMs, e.g., a microdisk. Second, introduce a one-parameter family of perturbations such that at least one HQM is almost unaffected and at least one HQM turns into a LQM having directed emission via refractive escape. Third, vary the parameter such that an avoided resonance crossing occurs between the HQM and the LQM. This scheme allows the systematic design of modes with high quality factors and highly directed emission.

This scheme has been demonstrated for the first time by a theoretical study of an annular cavity, a GaAs microdisk with a circular air hole [104]. Figure 11 shows for this system an avoided resonance crossing in the weak coupling regime, i.e. the frequencies cross and the quality factors repel each other. Both modes involved in this avoided crossing have even parity with respect to the symmetry axis. One mode has a high Q-value above $5 \cdot 10^5$, the other one has a low Q-value of ≈ 300 and unidirectional emission due to light reflection at the air hole. The hybridization is weak, which keeps the quality factors and the near-field patterns almost unaffected while the far-field pattern is in both cases dominated by the low-Q component; cf. the solid and dashed lines in Fig. 12. As a result a high-Q mode with unidirectional emission is obtained. This theoretical prediction has been confirmed in a recent experiment [108].

The problem of this particular system is the coexistence of even and odd symmetry modes. Since the scenario of avoided resonance crossings is in general different for the two symmetry classes, the respective output directionality may differ. In most of the practical cases both modes are involved in the process of light emission which then spoils the directionality. To avoid this problem of the mode coupling approach a less symmetric geometry is needed.

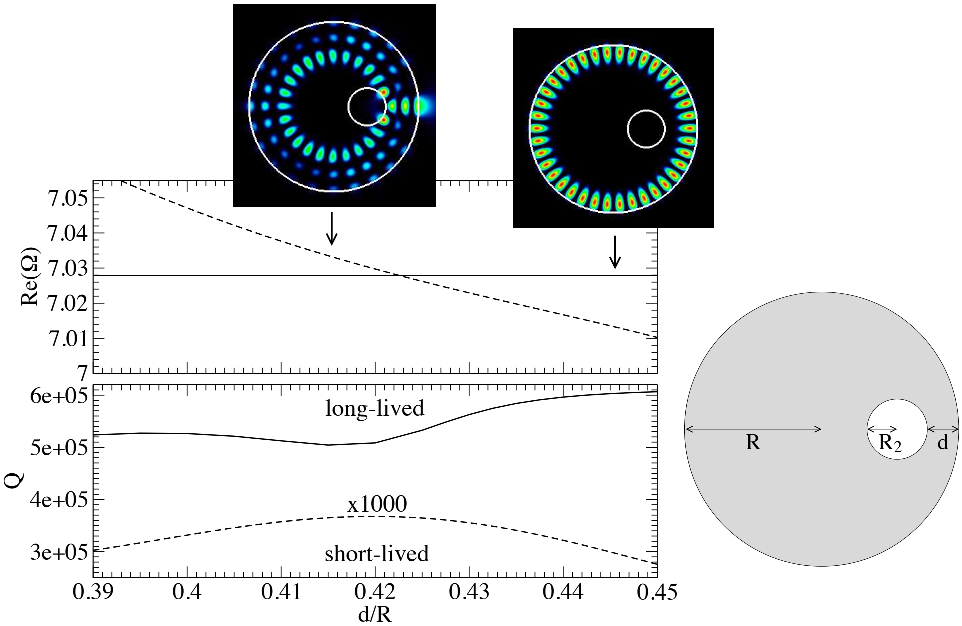

Figure 11: Normalized frequencies $\Omega = \omega R/c$ and quality factors vs. d for a high-Q WGM and a low-Q mode with directed emission in the annular cavity, a microdisk of radius R with an air hole of radius $R_2 = 0.22R$ located at the distance d to the disk's boundary. The index of refraction for TM polarization is $n = 3.3$.

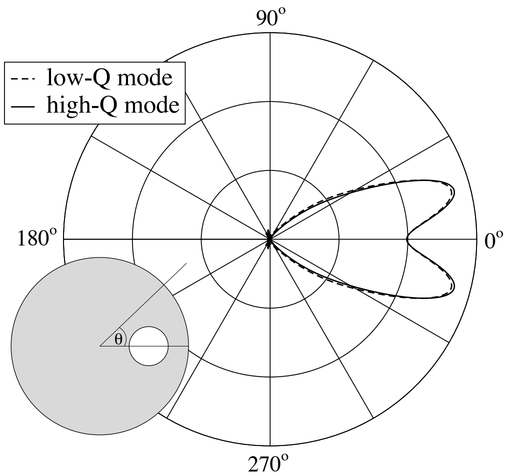

Figure 12: Far-field intensity pattern of the modes shown in Fig. 11 in the annular cavity.

8 Universal far-field pattern and the unstable manifold

In 2008 Wiersig and Hentschel proposed a new mechanism that produces unidirectional light emission and high quality factors simultaneously [109]. The key idea is to exploit light emission along unstable manifolds of the ray dynamics [110–113] to achieve unidirectional emission and to use wave localization such as scarring to get high Q-factors. Importantly, the output directionality is universal for all the high-Q modes because the corresponding escape routes of rays are similar. In experiments, this property enables one to robustly achieve unidirectional emission without any settings for selective excitation of specific modes.

The applicability of this idea was demonstrated for the cavity shape called the limaçon of Pascal defined by Eq. (2). In Fig. 13(a), ray simulations of far-field intensity patterns from the limaçon cavity are shown for the TE polarization (solid curve) and TM polarization (dashed curve). The choice of the deformation parameter ε and the effective index of refraction n of the cavity is important for obtaining unidirectional light emission. For $\varepsilon \approx 0.43$ and $n \approx 3.3$ (e.g. GaAs), one obtains optimal unidirectional light emission, while the unidirectionality is robust under small variations of these parameters.

For both TE and TM polarizations, we obtain (mostly) unidirectional emission patterns. The unidirectionality is better in the TE case than in the TM case. This difference was explained by the existence of the Brewster angle for the TE polarization in Ref. [109]. Figures 13(b) and (c) show the ray intensity distributions in the leaky phase-space region (i.e., $|\sin\chi| < 1/n$) for the TE case and for the TM case, respectively. These distributions describe how much ray intensity is emitted from a cavity boundary point s towards the direction specified by $\sin\chi$ (Snell's law implies the direction to be $\sin^{-1}(n\sin\chi)$) [82, 110, 112], and thus they can be regarded as near-field emission patterns taken just along the cavity boundary. The structures of these distributions are closely related to an invariant set of the ray dynamics, that is, the unstable manifolds emanating from the unstable periodic points located around the critical line for total internal reflection (i.e., $\sin\chi = \pm 1/n$) [110–113]. In Figs. 13(b) and (c), we also plot curves that are mapped to far-field angles $\theta = \text{const}$. Comparing these curves with the ray intensity distributions, one can confirm that rays are mainly emitted out to the far-field angles around $\theta = 0°$ with the divergence angle $\approx 30°$, which is consistent with the far-field patterns in Fig. 13(a). In the TM case

(Fig. 13(c)), there are significant ray intensities mapped to $\theta \approx 140^\circ$ and $\theta \approx 220^\circ$. This results in relatively larger sub-peaks around these far-field angles, which can be seen in Fig. 13(a). Owing to the ray-wave correspondence [114], solutions of the mode equation (1) for high-Q modes are supported on the ray intensity distributions, as we show later in Figs. 17(c) and (d). As a result, all high-Q modes exhibit unidirectional emission patterns closely corresponding to the ray calculation.

Soon after the theoretical proposal, several groups fabricated limaçon cavity lasers [115–118]. Song *et al.* studied GaAs limaçon cavities with the size parameter $R = 2.18\,\mu$m (dimensionless size parameter $n\omega R/c \approx 48$) by optical pumping [115], Shinohara *et al.* studied larger GaAs cavities with $R = 20$ to $50\,\mu m$ ($n\omega R/c \approx 480$ to 1200) by electric pumping with pulsed currents [116], while Yi *et al.* studied InGaAsP cavities with $R = 50\,\mu$m ($n\omega R/c \approx 650$) by electric pumping with continuous wave (cw) currents [118]. In all of these studies, measured light emissions are TE-polarized and highly unidirectional emissions closely corresponding to the ray simulations were confirmed. On the other hand, TM-polarized unidirectional emission was confirmed by Yan *et al.* for quantum cascade lasers with the limaçon cavities with $R = 80\,\mu$m ($n\omega R/c \approx 161$), where again close agreement with the ray simulations is reported [117].

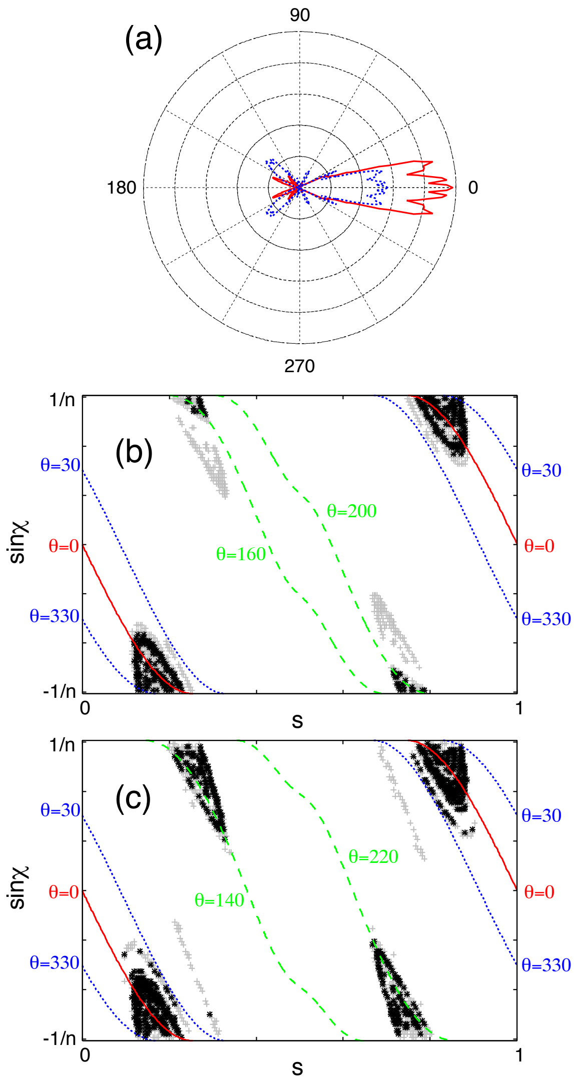

Figure 13: Ray simulations of unidirectional emission from a limaçon cavity with refractive index $n = 3.3$ and deformation parameter $\varepsilon = 0.43$. (a) Far-field intensity patterns are normalized so that the integrated intensity is unity. The solid (dashed) curve is for TE (TM) polarization. (b) and (c) are ray intensity distributions in the leaky phase-space region (i.e., $|\sin\chi| < 1/n$) for TE and for TM polarization, respectively, where curves mapped to far-field angles $\theta =$ const are superimposed. The intensity increases as the color changes from white to black. The arclength s is normalized to the cavity's perimeter.

Next we present, as an example, experimental results of lasing of InAs quantum dots (QDs) in limaçon-shaped GaAs microdisks in Ref. [115]. The inhomogeneously broadened gain spectrum of InAs QDs results in lasing in multiple modes well separated in wavelength. All the lasing modes have single output beam in the same direction, regardless of their wavelengths and intracavity mode structures. Our numerical simulations show two types of high-Q modes in the limaçon cavity: scar modes [109] and whispering-gallery-like modes. Unlike the former, the latter do not correspond to any closed ray orbits yet can have higher Q factors than the former.

Figure 14 shows the top-view and tilt-view scanning electron microscope (SEM) images of a GaAs microdisk fabricated by photolithography and wet chemical etching. The 265 nm-thick GaAs disk is on top of an $Al_{0.68}Ga_{0.32}As$ pedestal and contains six layers of InAs QDs. The disk boundary can be fitted well to a limaçon shape with $\epsilon = 0.45$ and $R = 2.18\,\mu$m.

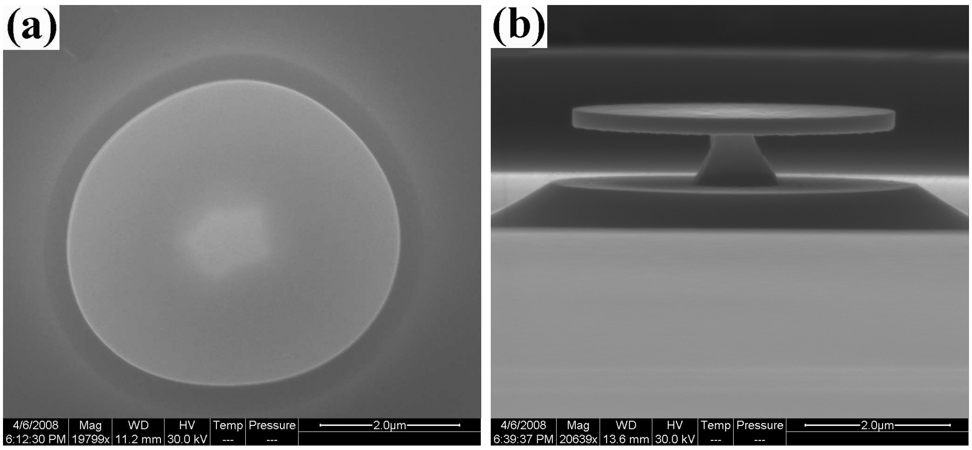

Figure 14: Scanning electron microscope images of a deformed GaAs microdisk on top of a $Al_{0.68}Ga_{0.32}As$ pedestal. (a) Top view, (b) tilt view. The GaAs disk is 265 nm thick and contains six layers of InAs QDs. The 1000 nm long $Al_{0.68}Ga_{0.32}As$ pedestal separates the GaAs disk from the substrate. To minimize its effect on lasing modes in the disk, the pedestal is etched to have a top lateral dimension of 620 nm.

The QDs are optically excited and provide gain for lasing in the microcavity. Figure 15(a) is part of a time-integrated emission spectrum, which consists of several narrow peaks. The inhomogeneously broadened gain spectrum of InAs QDs results in lasing in multiple modes well separated in wavelength. Figure 15(b) shows the intensity I and linewidth $\Delta\lambda$ of one peak at

$\lambda = 998$ nm as a function of the incident pump intensity P. The variation of $\log I$ with $\log P$ exhibits a S-shape with two kinks at $P \simeq 102$ W/cm^2 and 300 W/cm^2. The first kink corresponds to the transition from linear increase of I with P to superlinear increase. Since the superlinear increase is caused by light amplification, the first kink represents the onset of optical gain, i.e. the transparency threshold. Above the second kink the increase of I with P becomes linear again due to gain saturation. The linewidth drops rapidly with increasing P, eventually approaching the resolution of our spectrometer. These data demonstrate lasing in the limaçon cavity. We estimate the Q factor from the linewidth at the transparency threshold and obtained a value of 23000. It is significantly higher than all the previously reported Q values of deformed microcavities, in spite of smaller cavity size. The high quality factor and small modal volume result in very low lasing threshold, allowing continuous wave (cw) operation. The spontaneous emission coupling efficiency β, which represents the percentage of spontaneously emitted photons to the lasing mode, estimated from the threshold curve in Fig. 15(b) [119] (see also [3, 120]) is approximately 6%, which is comparable to typical nonchaotic microcavity lasers [121, 122]. β is usually larger for a microcavity of smaller size and higher quality factor. Since the previously realized chaotic microcavity lasers have lower Q and larger modal volume than the limaçon cavity, their β values shall be smaller. However, this is the first time that β has been reported for a chaotic microcavity.

The far-field pattern of laser emission from a limaçon cavity is obtained by scattering of in-plane output light by a large ring fabricated around each microdisk. Figure 16(a) is an optical image of laser emission from microdisk scattered by the ring. It shows the laser output from the limaçon cavity is predominately in one direction. As shown in Fig. 16(b), the output beam is centered around $\theta = 0$ with a width of 40°. The fraction of far-field emission was computed as a function of subtended angle. 68% of total emission intensity is confined within $|\theta| \leq 40°$, and about 50% of emission within $|\theta| \leq 20°$. The emission spectrum taken simultaneously with the image [Fig. 16(c)] reveals multi-mode lasing. Hence, the directional emission shown in Fig. 16(b) comes from all lasing modes. Figure 16(d) shows the far-field patterns of two lasing modes at wavelength 909 nm and 923 nm. They are similar to that of total laser emission except for a small variation in angular distribution of output intensity. Therefore, all the lasing modes have output beams in the same direction with similar divergence angle.

To understand the nature of lasing modes, we performed numerical simulations of actual microdisks that are measured. Since the pump intensity is uniform across the disk, the lasing modes correspond to high-Q TE res-

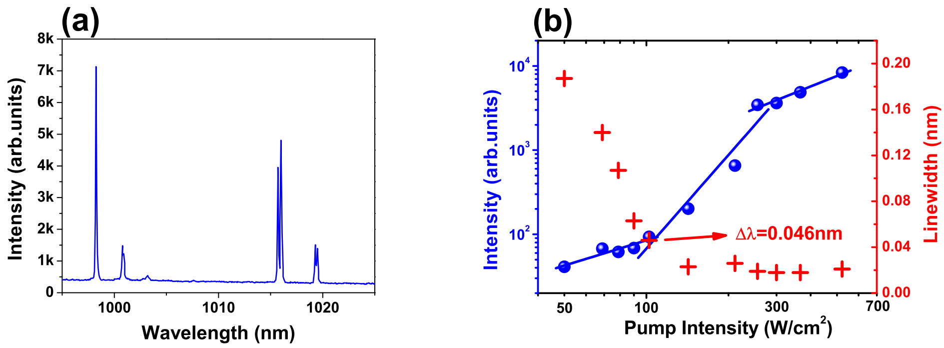

Figure 15: Experimental results of lasing in the limaçon microcavity under cw pumping. (a) Part of a time-integrated emission spectrum taken at the incident pump intensity $P = 522$ W/cm^2. It consists of several narrow peaks. (b) Intensity I (blue dots) and spectral width $\Delta\lambda$ (red crosses) of one peak at $\lambda = 998$ nm as a function of incident pump intensity P. The variation of $\log I$ with $\log P$ exhibits two kinks at which the slope changes. The blue solid lines represent linear fitting that gives the slope values. The slope is equal to 0.99 below the first kink, 3.68 between the first and second kinks, and 1.01 above the second kink.

onances, which we calculated by solving the Maxwell's equations with the FDTD method.

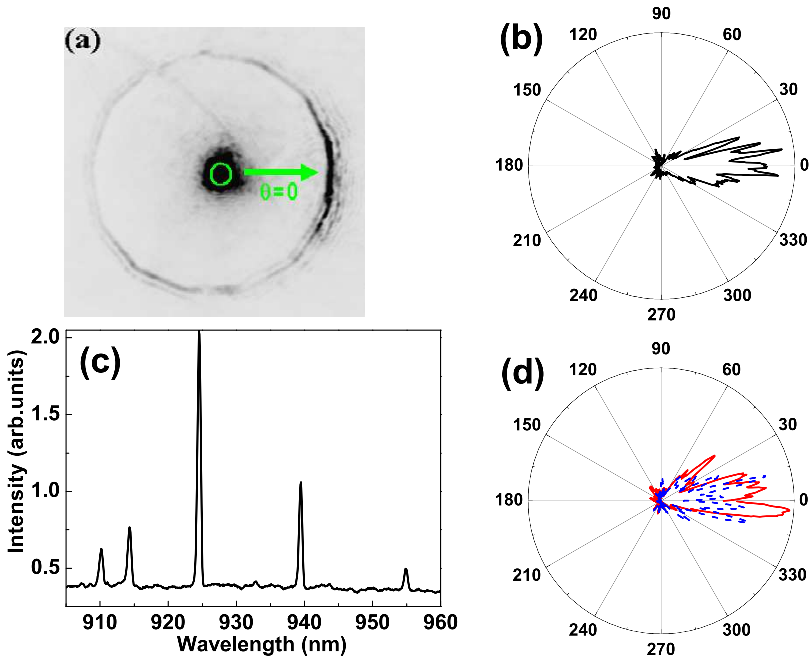

Figure 16: Measured directionality of laser emission from the limaçon microcavity pumped by 200 fs pulses of a mode-locked Ti:Sapphire laser. The incident pump power is $92\,\mathrm{W/cm^2}$. (a) An image of laser emission from the microdisk scattered by the ring surrounding the disk. The ring is centered at the disk and has a radius of $34\,\mu$m. Long integration time of the CCD camera, necessary to obtain a clear image of weak scattered light along the ring, causes an over-exposure of the disk itself. The disk boundary is drawn with green line. The polar angle $\theta = 0$ is defined in (a). (b) Far-field angular distributions of emission intensities of all lasing modes. (c) Time-integrated emission spectrum taken simultaneously with the far-field emission pattern. (d) Far-field angular distributions of two lasing modes at $\lambda = 909\,$nm (red line) and 923 nm (blue dashed line). All the lasing modes have output beams along $\theta = 0$ with a divergence angle of $40°$.

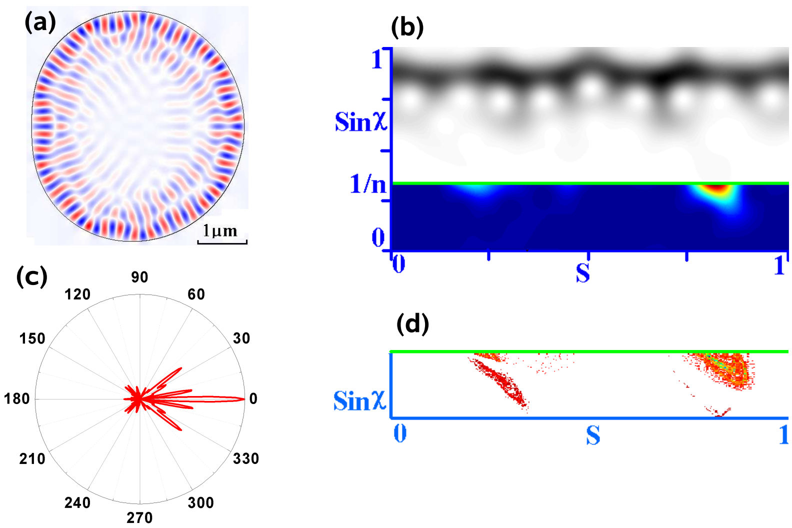

Figure 17: Numerical simulation results illustrating a WG-like high-Q mode in the experimentally measured limaçon microcavity. Calculated spatial intensity distributions (a) and Husimi function revealing the distributions of intensity and incident angle of light on the disk boundary (b), and far-field emission patterns (c) of the mode at $\lambda = 928$ nm. The horizontal axis of (c) represents the length along the disk boundary from the point $\theta = 0$ normalized by the cavity perimeter S, and the vertical axis corresponds to $\sin\chi$, where χ is the incident angle at the cavity boundary. (a,b) indicate the mode is like a WG mode. In (c) the intensities in the leaky region $|\sin\chi| < 1/n$ are enhanced to illustrate the escape route of light from the cavity. Panel (d) shows the distribution of optical ray amplitude in the leaky region obtained by classical ray tracing. The initial condition of ray simulation is 20,000 rays uniformly distributed above the critical line.

We found two types of high-Q modes in the limaçon cavity: (i) the scar modes as predicted by Wiersig and Hentschel [109]; and (ii) different WG-like modes. The second type of high-Q modes do not correspond to closed orbits like the scar modes, yet they have higher quality factor than the scar modes. Thus they are more likely to be the lasing modes because of lower lasing threshold. Figure 17(a) shows a simulation of one such mode at $\lambda = 928\,\text{nm}$. Its $Q = 94{,}000$, and $V_m = 0.19\,\mu\text{m}^3$. Figure 17(b) demonstrates that the intensity is distributed approximately uniformly along the cavity boundary, and the incident angle χ of light rays at the boundary is nearly constant. Thus, it is similar to a whispering-gallery (WG) mode. By integrating the mode intensity in Fig. 17(b) over the arclength s, we obtain its distribution in $\sin\chi$. The integrated intensity decays exponentially away from the maximal value at $\sin\chi_0 = 0.84$. The localization length, estimated from the decay length, is about 0.1. Since it is smaller than the distance (~ 0.52) from the mode center ($\sin\chi_0 = 0.84$) to the critical line ($\sin\chi_c = 0.32$), this mode is localized in the angular momentum $m = nkR\sin\chi$ [76–78]. Chaotic diffusion of rays towards lower χ is suppressed leading to the formation of WG-like mode. The exponentially small modal intensity in the leaky region (where $\sin\chi < 1/n$, and n is the refractive index of microdisk) results in extraordinarily high Q-factors. In real space the field intensity is very low in the disk center, avoiding Q degradation by scattering of the pedestal below the center of the disk. Although its intracavity mode structure is quite different from that of a scar mode, the far-field pattern is similar. As shown in Fig. 17(c), the WG-like mode has emission predominantly in the direction θ near 0. The color-enhanced intensity distribution in the leaky region [Fig. 17(b)] illustrates that the escape route of light from the cavity is identical to that of rays obtained by the ray tracing calculation in Fig. 17(d). It confirms the universal output directionality results from ray dynamics in the open cavity.

9 Wavelength-scale microdisks

Lately there has been a strong push towards further reduction of microlaser size for applications to nanophotonic circuits, on-chip optical interconnects, very local chemical and biological sensing. To avoid high optical bend losses in dielectric disks, most microdisk lasers have diameter over $1\,\mu\text{m}$ [123, 124]. In 2007 Zhang *et al.* realized submicron disk lasers which operate at room temperature and emit in the visible regime [125]. The smallest disks for

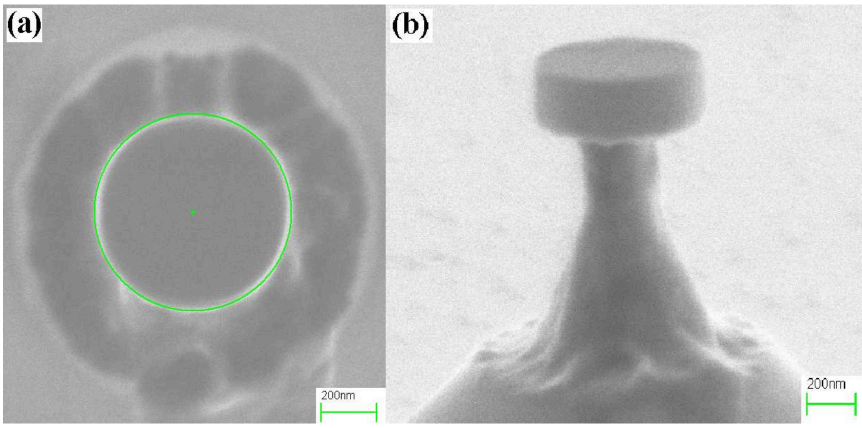

Figure 18: Top-view (a) and tilt-view (b) scanning electron microscope images of a GaAs disk on top of a AlGaAs pedestal. The disk diameter is 627 nm, and the disk thickness is 265 nm. The green circle is a fit of the disk shape.

which they achieved lasing operation have a diameter of 645 nm, which is equal to the lasing wavelength in vacuum. In 2009 Song *et al.* reported lasing in subwavelength GaAs disks at near-IR frequency [126]. The disks are fabricated by standard photolithography and two steps of wet chemical etching. The submicron disks have good circularity, a smooth boundary and a vertical sidewall. Single mode lasing is obtained by optical pumping. The gain is provided by the wetting layers of InAs QDs embedded in the GaAs disks. The diameter of the smallest lasing disks is 627 nm, which is about 30% smaller than the vacuum lasing wavelength [Fig. 18]. The disk thickness is 265 nm. Figure 19(a) shows the onset of lasing action at the incident pump power $P = 220\ \mu$W. The inset of Fig. 19(b) is the lasing spectrum featuring a single mode lasing at $\lambda = 870$ nm. A threshold behavior is clearly seen in the growth of peak intensity with pumping [Fig. 19(a)]. Figure 19(b) is a plot of the peak width $\Delta\lambda$ versus P. $\Delta\lambda$ first decreases with increasing P, then saturates at higher P. The minimal linewidth is about 1.7 nm. The 3D FDTD calculations show that the lasing mode is a WGM with the azimuthal number $m = 4$. The modal volume is $0.97\,(\lambda/n)^3$. This is the smallest dielectric disk laser that has been reported so far.

The model that is usually used to explain and predict the directional emission from various deformed microdisks is based on the ray optics, which breaks down as the wavelength approaches the cavity size. Since wave transport differs substantially from ray transport, the output directionality of the

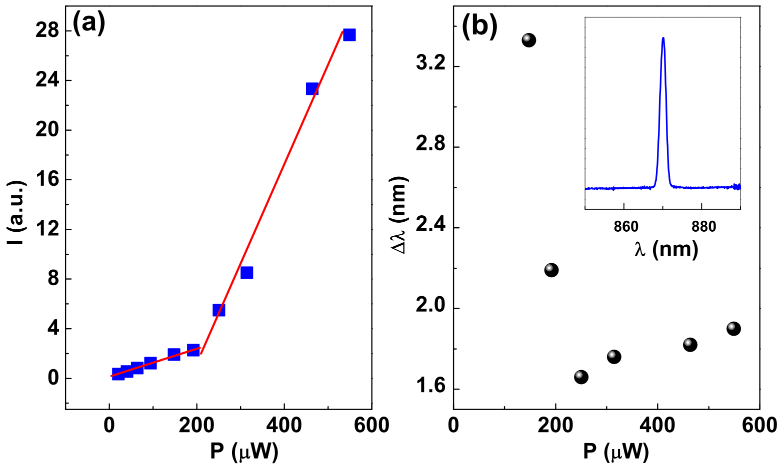

Figure 19: (a) Linear plot of the lasing peak intensity vs. the incident pump power P for the GaAs disk shown in Fig. 18. The straight lines are fitted curves. (b) Spectral width $\Delta\lambda$ of the lasing peak as a function of pump power P. Inset: the emission spectrum at $P = 300$ μW showing the lasing peak.

wavelength-scale or subwavelength cavities can be completely different from the prediction of the ray model. New physical mechanism shall be exploited to achieve simultaneously unidirectional emission and high-Q factor. It is a future challenge to develop the new design rule for the wavelength-scale deformed microdisks.

10 Summary

The quest to achieve directional radiation from microcavity lasers has stimulated a lot of activities in the field of optical microresonators and considerably deepened our understanding for them – by applying very different physical principles and mechanisms and by using theoretical concepts that were originally developed in other fields. As a result, a number of very different approaches were found and investigated, and many (but not all) of them are sketched here. For example, we left out the theoretical study [127, 128] that placed a point-scatterer in a circular cavity where it causes a lensing-type effect that collimates the light scattered at this defect. The ideas presented here comprise a broad range of concepts – from tailoring resonator shapes (such as in the limaçon microlasers) to mode interactions occurring at avoided resonance crossings (such as in the annular resonator) or an pumping-induced mode-beating interaction (such as in the spiral). They not only considerably enlarged our understanding of microlasers, but at the same time highlighted the role played by quantum chaos in such open systems. The recognition of the importance of the unstable manifold that explains, e.g., the observed universality of the far-field patterns, is one prominent example for this. In turn, based on this knowledge, new resonator shapes can now be deviced and easily (pre-)tested by ray simulations, which will tremendously help on the application side.

Although this review presents a number of possibilities how to achieve directional light-output from microlasers that comprise a big step towards the solution of this problem, new challenges are already visible ahead of us. They are related to the further miniaturisation of the devices that already nowadays reach the size of just a few wavelengths. Well-known wave corrections to the ray model, such as the Goos-Hänchen shift [129–131] and the Fresnel filtering effects [132–134], will then become important and lead to the expected deviations between the (conventional) ray-model predictions on the one hand, and wave simulations and experimental results on the other hand side. Such deviations have become visible recently and open a new route for both deeper theoretical insight and new manipulation mechanisms.

Another important question that one has to address is the design of cavity shapes allowing for unidirectional emission in the case of a low index of refraction. A first step in this direction has been done by Zou *et al.* [135].

Acknowledgments

Financial support from the DFG research group 760 and DFG Emmy Noether Programme is gratefully acknowledged.

References

[1] K. J. Vahala, "Optical microcavities", Nature (London) **424**, 839 (2003).

[2] H.-G. Park, S.-H. Kim, S.-H. Kwon, Y.-G. Ju, J.-K. Yang, J.-H. Baek, S.-B. Kim, and Y.-H. Lee, "Electrically Driven Single-Cell Photonic Crystal Laser", Science **305**, 1444 (2004).

[3] S. M. Ulrich, C. Gies, S. Ates, J. Wiersig, S. Reitzenstein, C. Hofmann, A. Löffler, A. Forchel, F. Jahnke, and P. Michler, "Photon statistics of semiconductor microcavity lasers", Phys. Rev. Lett. **98**, 043906 (2007).

[4] P. Michler, A. Imamoğlu, M. D. Mason, P. J. Carson, G. F. Strouse, and S. K. Buratto, "Quantum correlation among photons from a single quantum dot at room temperature", Nature (London) **406**, 968 (2000).

[5] J.P. Reithmaier, G. Sek, A. Löffler, C. Hofmann, S. Kuhn, S. Reitzenstein, L.V. Keldysh, V.D. Kulakovskii, T.L. Reinecke, and A. Forchel, "Strong coupling in a single quantum dot-semiconductor microcavity system", Nature (London) **432**, 197 (2004).

[6] E. Peter, P. Senellart, D. Martrou, A. Lemaitre, J. Hours, J. M. Gérard, and J. Bloch, "Exciton-Photon strong-coupling regime for a single quantum dot in a microcavity", Phys. Rev. Lett. **95**, 067401 (2005).

[7] M. Schwab, H. Kurtze, T. Auer, T. Berstermann, M. Bayer, J. Wiersig, N. Baer, C. Gies, F. Jahnke, J.P. Reithmaier, A. Forchel, M. Benyoucef, and P. Michler, "Radiative emission dynamics of quantum dots in a single cavity micropillar", Phys. Rev. B **74**, 045323 (2006).

[8] J. Wiersig, C. Gies, F. Jahnke, M. Aßmann, T. Berstermann, M. Bayer, C. Kistner, S. Reitzenstein, C. Schneider, S. Höfling, A. Forchel, C. Kruse, J. Kalden, and D. Hommel, "Direct observation of correlations between individual photon emission events of a microcavity laser", Nature **460**, 245 (2009).

[9] S. L. McCall, A. F. J. Levi, R. E. Slusher, S. J. Pearton, and R. A. Logan, "Whispering-gallery mode microdisk lasers", Appl. Phys. Lett. **60**, 289 (1992).

[10] C. P. Michael, K. Srinivasan, T. J. Johnson, O. Painter, K. H. Lee, K. Hennessy, H. Kim, and E. Hu, "Wavelength- and material-dependent absorption in GaAs and AlGaAs microcavities", Appl. Phys. Lett. **90**, 051108 (2007).

[11] T. J. Kippenberg, J. Kalkman, A. Polman, and K. J. Vahala, "Demonstration of an erbium-doped microdisk laser on a silicon chip", Phys. Rev. A **74**, 051802(R) (2006).

[12] A. C. Tamboli, E. D. Haberer, R. Sharma, K. W. Lee, S. Nakamura, and E. L. Hu, "Room-temperature continuous-wave lasing in GaN/InGaN microdisks", Nature Photonics **1**, 61 (2007).

[13] L. Collot, V. Lefevre-Seguin, M. Brune, J.M. Raimond, and S. Haroche, "Very high Q whispering gallery modes observed on fused silica microspheres", Europhys. Lett. **23**, 327 (1993).

[14] M. L. Gorodetsky, A. D. Pryamikov, and V. S. Ilchenko, "Rayleigh scattering in high-Q microsphere", J. Opt. Soc. Am B **17**, 1051 (2000).

[15] S. Götzinger, L. de S. Menezes, A. Mazzei, S. Kühn, V. Sandoghdar, and O. Benson, "Controlled photon transfer between two individual nanoemitters via shared high-Q modes of a microsphere resonator", Nano Lett. **6**, 1151 (2006).

[16] V. S Ilchenko, M. L. Gorodetsky, X. S. Yao, and L. Maleki, "Microtorus: a high-finesse microcavity with whispering-gallery modes", Opt. Lett. **26**, 256 (2001).

[17] D. K. Armani, T. J. Kippenberg, S. M. Spillane, and K. J. Vahala, "Ultra-high-Q toroid microcavity on a chip", Nature **421**, 925 (2003).

[18] A. A. Savchenkov, V. S. Ilchenko, A. B. Matsko, and L. Maleki, "Kilohertz optical resonances in dielectric crystal cavities", Phys. Rev. A **70**, 051804(R) (2004).

[19] H. Lohmeyer, K. Sebald, J. Gutowski, R. Kröger, C. Kruse, D. Hommel, J. Wiersig, and F. Jahnke, "Resonant modes in monolithic nitride pillar microcavities", Eur. Phys. J B **48**, 291 (2005).

[20] A. F. J. Levi, R. E. Slusher, S. L. McCall, J. L. Glass, S. J. Pearton, and R. A. Logan, "Directional light coupling from microdisk lasers", Appl. Phys. Lett. **62**, 561 (1993).

[21] J. U. Nöckel and A. D. Stone, "Chaos in optical cavities", Nature (London) **385**, 45 (1997).

[22] C. Gmachl, F. Capasso, E. E. Narimanov, J. U. Nöckel, A. D. Stone, J. Faist, D. L. Sivco, and A. Y. Cho, "High-Power Directional Emission from Microlasers with Chaotic Resonators", Science **280**, 1556 (1998).

[23] T. Tanaka, M. Hentschel, T. Fukushima, and T. Harayama, "Classical Phase Space Revealed by Coherent Light", Phys. Rev. Lett. **98**, 033902 (2007).

[24] G. D. Chern, H. E. Tureci, A. D. Stone, R. K. Chang, M. Kneissl, and N. M. Johnson, "Unidirectional lasing from InGaN multiple-quantum-well spiral-shaped micropillars", Appl. Phys. Lett. **83**, 1710 (2003).

[25] M. S. Kurdoglyan, S.-Y. Lee, S. Rim, and C.-M Kim, "Unidirectional lasing from a microcavity with a rounded isoceles triangle shape", Opt. Lett. **29**, 2758 (2004).

[26] M. Kneissl, M. Teepe, N. Miyashita, N. M. Johnson, G. D. Chern, and R. K. Chang, "Current-injection spiral-shaped microcavity disk laser diodes with unidirectional emission", Appl. Phys. Lett. **84**, 2485 (2004).

[27] J. U. Nöckel, A. D. Stone, and R. K. Chang, "Q spoiling and directionality in deformed ring cavities", Opt. Lett. **19**, 1693 (1994).

[28] J. D. Jackson, *Classical Electrodynamics* (John Wiley and Sons, New York, 1962).

[29] A. Taflove and S. C. Hagness, *Computational Electrodynamics the Finite-Difference Time-Domain Method* (Artech House, London, 2000).

[30] J. Förstner, Dissertation, Technische Universität Berlin, 2005.

[31] W. Fang, A. Yamilov, and H. Cao, "Analysis of high-quality modes in open chaotic microcavities", Phys. Rev. A **72**, 023815 (2005).

[32] W. Fang, H. Cao, and G. S. Solomon, "Control of lasing in fully chaotic open microcavities by tailoring the shape factor", Appl. Phys. Lett. **90**, 081108 (2007).

[33] W. Fang and H. Cao, "Wave interference effect on polymer microstadium laser", Appl. Phys. Lett. **91**, 041108 (2007).

[34] J. U. Nöckel and A. D. Stone, in *Optical Processes in Mircocavities*, Vol. 3 of *Advanced Series in applied Physics*, edited by R. K. Chang and A. J. Campillo (World Scientific, Singapore, 1995).

[35] G. Chen and J. Zhou, *Boundary element methods* (Academic Press, San Diego, 1992).

[36] P. K. Banerjee, *The boundary element methods in engineering* (McGraw-Hill, London, 1994).

[37] J. Wiersig, "Boundary element method for resonances in dielectric microcavities", J. Opt. A: Pure Appl. Opt. **5**, 53 (2003).

[38] O. J. F. Martin, A. Dereux, and C. Girard, "Iterative scheme for computing exactly the total field propagating in dielectric structures of arbirary shape", J. Opt. Soc. Am. A **11**, 1073 (1994).

[39] O. J. F. Martin, C. Girard, and A. Dereux, "Generalized field propagator for electromagnetic scattering and light confinement", Phys. Rev. Lett. **74**, 526 (1995).

[40] A. Hoekstra, J. Rahola, and P. Sloot, "Accuracy of internal fields in volume integral equation simulations of light scattering", Appl. Opt. **37**, 8482 (1998).

[41] O. J. F. Martin, C. Girard, D. R. Smith, and S. Schultz, "Generalized field propagator for arbitrary finite-size photonic band gap structures", Phys. Rev. Lett. **82**, 315 (1999).

[42] J. U. Nöckel, Ph.D. thesis, Yale University, 1997.

[43] M. C. Gutzwiller, *Chaos in Classical and Quantum Mechanics*, Vol. 1 of *Interdisciplinary Applied Mathematics* (Springer, Berlin, 1990).

[44] F. Haake, *Quantum Signatures of Chaos* (Springer, Berlin, 1991).

[45] L. E. Reichl, *The Transition to Chaos in Conservative Classical Systems: Quantum Manifastations* (Springer, Berlin, 1992).

[46] H.-J. Stöckmann, *Quantum Chaos* (Cambridge University Press, Cambridge, UK, 2000).

[47] M. V. Berry, "Regularity and chaos in classical mechanics, illustrated by three deformations of a circular 'billiard"', Eur. J. Phys. **2**, 91 (1981).

[48] M. V. Berry, "Quantizing a classically ergodic system: Sinai's billiard and the KKR method", Ann. Phys. **131**, 163 (1981).

[49] M. Robnik, "Classical dynamics of a family of billiards with analytic boundaries", J. Phys. A **16**, 3971 (1983).

[50] M. Robnik, "Quantising a generic family of billiards with analytic boundaries", J. Phys. A **17**, 1049 (1984).

[51] V. V. Kozlov and D. V. Treshchev, *Billiards – A Genetic Introduction to the Dynamics of Systems with Impacts* (American Mathematical Society, Providence, RI, 1991).

[52] A. Bäcker, F. Steiner, and P. Stifter, "Spectral Statistics in the Quantized Cardioid Billiard", Phys. Rev. E **52**, 2463 (1995).

[53] H. Waalkens, J. Wiersig, and H. R. Dullin, "The Elliptic Quantum Billiard", Ann. Phys. (New York) **260**, 50 (1997).

[54] C. Dembowski, H.-D. Gräf, A. Heine, R. Hofferbert, H. Rehfeld, and A. Richter, "First experimental evidence for chaos-assisted tunneling in a microwave annular billiard", Phys. Rev. Lett. **84**, 867 (2000).

[55] J. Wiersig, "Singular continuous spectra in a pseudointegrable billiard", Phys. Rev. E **62**, R21 (2000).

[56] J. Nagler, M. Krieger, M. Linke, J. Schönke, and J. Wiersig, "Leaking billiards", Phys. Rev. E **75**, 046204 (2007).

[57] L. A. Bunimovich, "On Ergodic Properties of Certain Billiards", Funct. Anal. Appl. **8**, 254 (1974).

[58] K. F. Huang, Y. F. Chen, H. C. Lai, and Y. P. Lan, "Observation of the wave function of a quantum billiard from the transverse patterns of vertical-cavity surface-emitting lasers", Phys. Rev. Lett. **89**, 224102 (2002).

[59] T. Gensty, K. Becker, I. Fischer, W. Elsäßer, C. Degen, P. Debernardi, and G. P. Bava, "Wave chaos in real-world vertical-cavity surfaces-emitting lasers", Phys. Rev. Lett. **94**, 233901 (2005).

[60] S. Lacey and H. Wang, "Directional emission from whispering-gallerey modes in deformed fused-silica microspheres", Opt. Lett. **26**, 1943 (2001).

[61] S. Lacey, H. Wang, D. H. Foster, and J. U. Nöckel, "Directional tunneling escape from nearly spherical optical resonators", Phys. Rev. Lett. **91**, 033902 (2003).

[62] R. E. Slusher, A. F. J. Levi, U. Mohideen, S. L. McCall, S. J. Pearton, and R. A. Logan, "Threshold characteristics of semiconductor microdisk lasers", Appl. Phys. Lett. **63**, 1310 (1993).

[63] U. Mohideen, R. E. Slusher, F. Jahnke, and S. W. Koch, "Semiconductor Microlaser Linewidths", Phys. Rev. Lett. **73**, 1785 (1994).

[64] Lord Rayleigh, *The Theory of Sound* (American edition: Dover, New York, 1945), first published 1877.

[65] A. J. Lichtenberg and M. A. Lieberman, *Regular and Chaotic Dynamics* (Springer, Berlin, 1992).

[66] V. I. Arnol′d, *Mathematical Methods of Classical Mechanics*, Vol. 60 of *Graduate Texts in Mathematics* (Springer, Berlin, 1978).

[67] J. Nöckel, A. D. Stone, G. Chen, H. L. Grossman, and R. K. Chang, "Directional emission from asymmetric resonant cavities", Opt. Lett. **21**, 1609 (1996).

[68] M. Lebental, J. S. Lauret, R. Hierle, and J. Zyss, "Highly-directional stadium-shaped polymer microlasers", Appl. Phys. Lett. **88**, 031108 (2006).

[69] M. Lebental, J. S. Lauret, J. Zyss, C. Schmit, and E. Bogomolny, "Directional emission of stadium-shaped microlasers", Phys. Rev. A **75**, 033806 (2007).

[70] A. Bäcker, PhD thesis, Universität Ulm, 1998.

[71] A. N. Kolmogorov, "The conservation of conditionally periodic motions with a small variation in the Hamiltonian", Dokl. Akad. Nauk SSSR **98**, 527 (1954).

[72] V. I. Arnol′d, "Small denominators and problems of stability of motion in classical and celestial mechanics", Russ. Math. Surveys **18**, 85 (1963).

[73] J. Moser, "On invariant curves of area-preserving mappings of an annulus", Nachr. Akad. Wiss. Gött., Math. Phys. Kl.II 1 (1962).

[74] S. Fishmann, D. R. Grempel, and R. E. Prange, "Chaos, Quantum Recurrences, and Anderson Localization", Phys. Rev. Lett. **49**, 509 (1982).

[75] K. M. Frahm and D. L. Shepelyansky, "Quantum Localization in Rough Billiards", Phys. Rev. Lett. **78**, 1440 (1997).

[76] O. A. Starykh, P. R. J. Jacquod, E. E. Narimanov, and A. D. Stone, "Signature of dynamical localization in the resonance width distribution of wave chaotic cavities", Phys. Rev. E **62**, 2078 (2000).

[77] V. A. Podolskiy, E. Narimanov, W. Fang, and H. Cao, "Chaotic microlasers based on dynamical localization", Proceedings of Nat. Acad. of Sci. USA **101**, 10498 (2004).

[78] W. Fang, H. Cao, V.A. Podolskiy, and E.E. Narimanov, "Dynamical localization in microdisk lasers", Opt. Express **13**, 5641 (2005).

[79] E. J. Heller, "Bound-states eigenfunctions of classically chaotic Hamiltonian systems: Scars of periodic orbits", Phys. Rev. Lett. **53**, 1515 (1984).

[80] S. B. Lee, J. H. Lee, J. S. Chang, H. J. Moon, S. W. Kim, and K. An, "Observation of Scarred Modes in Asymmetrically Deformed Microcylinder Lasers", Phys. Rev. Lett. **88**, 033903 (2002).

[81] N. B. Rex, H. E. Tureci, H. G. L. Schwefel, R. K. Chang, and A. D. Stone, "Fresnel Filtering in Lasing Emission from Scarred Modes of Wave-Chaotic Optical Resonators", Phys. Rev. Lett. **88**, 094102 (2002).

[82] S.-Y. Lee, S. Rim, J.-W. Ryu, T.-Y. Kwon, M. Choi, and C.-M Kim, "Quasiscarred resonances in a spiral-shaped microcavity", Phys. Rev. Lett. **93**, 164102 (2004).

[83] T. Fukushima, T. Harayama, and J. Wiersig, "Ray-wave correspondence in an unstable quasistadium laser resonator", Phys. Rev. A **73**, 023816 (2006).

[84] M. J. Davis and E. J. Heller, "Quantum dynamical tunneling in bound states", J. Chem. Phys. **75**, 246 (1981).

[85] G. Hackenbroich and J. U. Nöckel, "Dynamical tunneling in optical cavities", Europhys. Lett. **39**, 371 (1997).

[86] A. Bäcker, R. Ketzmerick, S. Löck, J. Wiersig, and M. Hentschel, "Quality factors and dynamical tunneling in annular microcavities", Phys. Rev. A **79**, 063804 (2009).

[87] S. Shinohara, T. Harayama, T. Fukushima, M. Hentschel, T. Sasaki, and E. E. Narimanov, "Chaos-assisted directional light emission from microcavity lasers", Phys. Rev. Lett. **104**, 163902 (2010).

[88] S. Tomsovic and D. Ullmo, "Chaos-assisted tunneling", Phys. Rev. E **50**, 145 (1994).

[89] V.A. Podolskiy and E.E. Narimanov, "Semiclassical description of chaos-assisted tunneling", Phys. Rev. Lett. **91**, 263601 (2003).

[90] V.A. Podolskiy and E.E. Narimanov, "Chaos-assisted tunneling in dielectric microcavities", Opt. Lett. **30**, 474 (2005).

[91] G. D. Chern, H. E. Tureci, A. D. Stone, R. K. Chang, M. Kneissl, and N. M. Johnson, "Unidirectional lasing InGaN multiple-quantum-well spiral-shaped micropillars", Appl. Phys. Lett. **83**, 1710 (2003).

[92] J. Wiersig, "Reciprocal transmissions and asymmetric modal distributions in waveguide-coupled spiral-shaped microdisk resonators: Comment", Opt. Express **16**, 5874 (2008).

[93] J. Wiersig, S. W. Kim, and M. Hentschel, "Asymmetric scattering and nonorthogonal mode patterns in optical microspirals", Phys. Rev. A **78**, 053809 (2009).

[94] R. Audet, M. A. Belkin, J. A. Fan, B. G. Lee, K. Lin, and F. Capasso, "Single-mode laser action in quantum cascade lasers with spiral-shaped chaotic resonators", Appl. Phys. Lett. **91**, 131106 (2007).

[95] M. Hentschel, T.-Y. Kwon, M. A. Belkin, R. Audet, and F. Capasso, "Angular emission characteristics of quantum cascade spiral microlasers", Opt. Express **17**, 10335 (2009).

[96] M. Hentschel and T.-Y. Kwon, in *Complex Phenomena in Nanoscale Systems*, edited by G. Casati and D. Matrasulov (Springer, Berlin, 2009).

[97] M. Hentschel and T.-Y. Kwon, "Designing and understanding directional emission from spiral microlasers", Opt. Lett. **34**, 163 (2009).

[98] T. Harayama, P. Davis, and K. S. Ikeda, "Stable oscillations of a spatially chaotic wave function in a microstadium laser", Phys. Rev. Lett. **90**, 063901 (2003).

[99] T. Harayama, T. Fukushima, S. Sunada, and K. S. Ikeda, "Asymmetric stationary lasing patterns in 2D symmetric microcavities", Phys. Rev. Lett. **91**, 073903 (2003).

[100] M. Hentschel, Q. J. Wang, C. Yan, F. Capasso, T. Edamura, and H. Kan, "Emission properties of electrically pumped triangular shaped microlasers", to appear in Opt. Express (2010).

[101] H. G. L. Schwefel, Ph.D. thesis, Yale University, 2004.

[102] Y. Baryshnikov, P. Heider, W. Parz, and V. Zharnitsky, "Whispering-gallery modes inside asymmetric resonant cavities", Phys. Rev. Lett. **93**, 133902 (2004).

[103] J. Gao, P. Heider, C. J. Chen, X. Yang, C. A. Husko, and C. W. Wong, "Observations of interior whispering-gallery modes in asymmetric optical resonators with rational caustics.", Appl. Phys. Lett. **91**, 181101 (2007).

[104] J. Wiersig and M. Hentschel, "Unidirectional light emission from high-Q modes in optical microcavities", Phys. Rev. A **73**, 031802(R) (2006).

[105] J. von Neumann and E. P. Wigner, "Über das Verhalten von Eigenwerten bei adiabatischen Prozessen", Z. Phys. **30**, 467 (1929).

[106] W. D. Heiss, "Repulsion of resonance states and exceptional points", Phys. Rev. E **61**, 929 (2000).

[107] T. Timberlake and L. E. Reichl, "Changes in Floquet-state structure at avoided crossings: delocalization and harmonic generation", Phys. Rev. A **59**, 2886 (1999).

[108] F. Wilde, PhD thesis, Universität Hamburg, 2008.

[109] J. Wiersig and M. Hentschel, "Combining directional light output and ultralow loss in deformed microdisks", Phys. Rev. Lett. **100**, 033901 (2008).

[110] H. G. L. Schwefel, N. B. Rex, H. E. Tureci, R. K. Chang, and A. D. Stone, "Dramatic shape sensitivity of directional emission patterns from similarly deformed cylindrical polymer lasers", J. Opt. Soc. Am. B **21**, 923 (2004).

[111] S.-Y. Lee, J.-W. Ryu, T.-Y. Kwon, S. Rim, and C.-M Kim, "Scarred resonances and steady probability distribution in a chaotic microcavity", Phys. Rev. A **72**, 061801(R) (2005).

[112] S. Shinohara, T. Harayama, H. E. Tureci, and A. D. Stone, "Ray-wave correspondence in the nonlinear description of stadium-cavity lasers", Phys. Rev. A **74**, 033820 (2006).

[113] S.-B. Lee, J. Yang, S. Moon, J.-H. Lee, K. An, J.-B. Shim, H.-W. Lee, and S. W. Kim, "Universal output directionality of single modes in a deformed microcavity", Phys. Rev. A **75**, 011802(R) (2007).

[114] S. Shinohara and T. Harayama, "Signature of ray chaos in quasi-bound wavefunctions for a stadium-shaped dielectric cavity", Phys. Rev. E **75**, 036216 (2007).

[115] Q. Song, W. Fang, B. Liu, S. T. Ho, G. S. Solomon, and H. Cao, "Chaotic Microcavity Laser with Low Threshold and Unidirectional Output", Phys. Rev. A **80**, 041807(R) (2009).

[116] S. Shinohara, M. Hentschel, J. Wiersig, T. Sasaki, and T. Harayama, "Ray-wave correspondence in limaçon-shaped semiconductor microcavities", Phys. Rev. A **80**, 031801(R) (2009).

[117] C. Yan, Q. J. Wang, L. Diehl, M. Hentschel, J. Wiersig, N. Yu, Pflügel, M. A. Belkin, T. Edamura, M. Yamanishi, H. Kan, and F. Capasso, "Directional light emission from microcavity quantum cascade lasers with limaçon-shaped resonator", Appl. Phys. Lett. **94**, 251101 (2009).

[118] C.-H. Yi, M.-W. Kim, and C.-M. Kim, "Lasing characteristics of a Limaçon-shaped microcavity laser", Appl. Phys. Lett. **95**, 141107 (2009).

[119] G. Bjork, H. Heitmann, and Y. Yamamoto, "Spontaneous-emission coupling factor and mode characteristics of planar dielectric microcavity lasers", Phys. Rev. A **47**, 4451 (1993).

[120] C. Gies, J. Wiersig, and F. Jahnke, "Output Characteristics of Pulsed and Continuous-Wave-Excited Quantum-Dot Microcavity Lasers", Phys. Rev. Lett. **101**, 067401 (2008).

[121] K. Srinivasan, M. Borselli, and O. Painter, "Cavity Q, mode volume, and lasing threshold in small diameter AlGaAs microdisks with embedded quantum dots", Opt. Express **14**, 1094 (2006).

[122] H. Takashima, H. Fujiwara, S. Takeuchi, K. Sasaki, and M. Takahashi, "Control of spontaneous emission coupling factor beta in fiber-coupled microsphere resonators", Appl. Phys. Lett. **92**, 071115 (2008).

[123] A. F. J. Levi, S. L. McCall, S. J. Pearton, and R. A. Logan, "Room-temperature operation of submicrometer radius disk laser", Electron. Lett. **29**, 1666 (1993).

[124] T. Baba, "Photonic crystals and microdisk cavities based on GaInAsP-InP system", IEEE J. Select. Topics Quantum Electron. **3**, 808 (1997).

[125] Z. Y. Zhang, L. Yang, V. Liu, T. Hong, K. Vahala, and A. Scherer, "Visible submicron microdisk lasers", Appl. Phys. Lett. **90**, 111119 (2007).

[126] Q. Song, H. Cao, S. T. Ho, and G. S. Solomon, "Near-IR subwavelength microdisk lasers", Appl. Phys. Lett. **94**, 061109 (2009).

[127] C. P. Dettmann, G. V. Morozov, M. Sieber, and H. Waalkens, "Directional emission from an optical microdisk resonators with a point scatterer", Europhys. Lett. **82**, 34002 (2008).

[128] C. P. Dettmann, G. V. Morozov, M. Sieber, and H. Waalkens, "Unidirectional emission from circular dielectric microresonators with a point scatterer", Phys. Rev. A **80**, 063813 (2009).

[129] F. Goos and H. Hänchen, "Ein neuer und fundamentaler Versuch zur Totalreflexion", Ann. Phys. (Leipzig) **1**, 333 (1947).

[130] M. Hentschel and H. Schomerus, "Fresnel laws at curved dielectric interfaces of microresonators", Phys. Rev. E **65**, 045603(R) (2002).

[131] J. Unterhinninghofen, J. Wiersig, and M. Hentschel, "Goos-Hänchen shift and localization of optical modes in deformed microcavities", Phys. Rev. E **78**, 016201 (2008).

[132] H. E. Tureci and A. D. Stone, "Deviation from Snell's law for beams transmitted near the critical angle: application to microcavity lasers", Opt. Lett. **27**, 7 (2002).

[133] H. Schomerus and M. Hentschel, "Correcting Ray Optics at Curved Dielectric Microresonator Interfaces: Phase-Space Unification of Fresnel Filtering and the Goos-Hänchen Shift", Phys. Rev. Lett. **96**, 243903 (2006).

[134] E. G. Altmann, G. Del Magno, and M. Hentschel, “Non-Hamiltonian dynamics in optical microcavities resulting from wave-inspired corrections to geometric optics”, Europhys. Lett. **84**, 10008 (2008).

[135] C.-L. Zou, F.-W. Sun, C.-H. Dong, X.-W. Wu, J.-M. Cui, Y. Yang, G.C. Guo, and Z.-F Han, “Mechanism of unidirectional emission of ultrahigh Q whispering gallery mode in microcavities”, arXiv:0908.3531 (2009).